

CFD modelling of highly viscous polymer thin film flow on a vertically rotational disk partially immersed in liquid for synthesis of polyethyleneterephthalat

Md Salim Miah^a, Christian Dassler^b, Xiaogang Yang^{*a}, Jianguang Hu^c

^aInstitute for Arts, Science and Technology

Glyndŵr University, Wrexham, LL11 2AW, UK

^bMobility Systems Division, Schaeffler Technologies AG & Co. KG

Industriestrasse 1-3, 91074 Herzogenaurach, Germany

^cState Key Laboratory of Chemical Engineering, East China University of Science and Technology

130 Meilong Road, Shanghai, 200237 P.R. China

*Corresponding Author's E-mail Address: x.yang@glyndwr.ac.uk

ABSTRACT

The present study focuses on liquid thin film flows on vertically rotational disk that is partially immersed in a liquid bath. This paper aims to investigate the liquid thin film flow on a rotational disk using CFD modelling approach and employing the mathematical model as proposed by Afanasiev *et. al.* [1], and to define the stability and shapes of the thin film thickness profiles. The dominant factors that determine the film thickness are identified with proposing a correlation equation to predict the film thickness as a function of angular position, radius, rotating speed, viscosity and surface tension. The thin film thickness variation in the angular direction (θ) and the film dragged into the liquid are particularly investigated since they have been overlooked in previously documented researches.

INTRODUCTION

Thin film flows are encountered in a wide range of industrial applications [2,3]. An example is the synthesis of polyethyleneterephthalat (PET) in polycondensation reactors in which a series of vertically rotational disks are partially immersed in highly viscous polymer liquid, thus picking up and spreading the melt in the form of thin film on the surface of the disks. Unlike the thin film flow on a horizontally rotational disk, the thin film flow on a vertically rotational disk partially immersed in liquid is always associated with a meniscus region where the liquid is dragged out by the disk moving and a specially oscillating region where the film formed on the disk is dragged into the liquid. While a lot of studies on the thin flow on horizontal rotational disk have been documented in the open literature, there have been limited studies on vertical setup and the fluid dynamical aspects are still not fully understood although there are some discussion and general solutions of film thickness profiles for the problem of liquid drag out [4, 5]. In this research the proposed mathematical model by Afanasiev

et.al. (2008) is further extended to define the film pattern formed on the vertically rotational disk and Volume of Fluid (VOF) method is employed for solving this kind of problem using CFD code – ANSYS Fluent. For the problem of the film formation on the vertically rotating disk partially immersed in liquid, the force balance is important as the shape and stability of the thin film is controlled by various forces acting on it including viscous, inertial, surface tension, centrifugal, coriolis and gravitational forces. For a vertically rotating disk the coriolis force can be neglected at the leading order as the term of the coriolis force has the same order as the terms of the inertial forces due to the restriction of the lubrication theory [6, 7, 8].

NOMENCLATURE

Ca	[-]	Capillary number
D	[m]	Immersion depth
d'	[-]	Dimensionless immersion depth
Fr	[-]	Froude number
G	[m/s ²]	Gravitational acceleration
H	[m]	Thin film thickness
h'	[-]	Dimensionless film thickness
R	[m]	Disk radius
R'	[-]	Dimensionless disk radius
Re	[-]	Reynolds number
T	[s]	Time
We	[-]	Webber number

Special characters

α	[-]	Aspect ratio of the flow
θ	[°]	Angular coordinate
Ω	[rpm]	Rotating speed
ν	[m ² /s]	Kinematic viscosity
ρ	[kg/m ³]	Density
μ	[Pa.s]	Dynamic viscosity
σ	[N/m]	Surface tension
ω	[rad/s]	Angular velocity

Subscripts

CFD	Computational fluid dynamics
CFL	Courant-Friedrich-Lewy number

MATHEMATICAL MODELLING

The physical set up for the vertically rotating disk partially immersed in liquid is shown in Figure 1. A disk of radius R is rotating at the angular velocity Ω about its horizontal axis which has a distance d to the liquid bath. For most of thin film flows on vertically rotating disks, the flows can be treated as incompressible. For the problem of the vertically rotating disk, cylindrical coordinate system is employed for convenience. Let the liquid velocity vector to be represented by (u_r, u_θ, u_z) and ω denotes the angular velocity vector with components $(0, 0, \Omega)$.

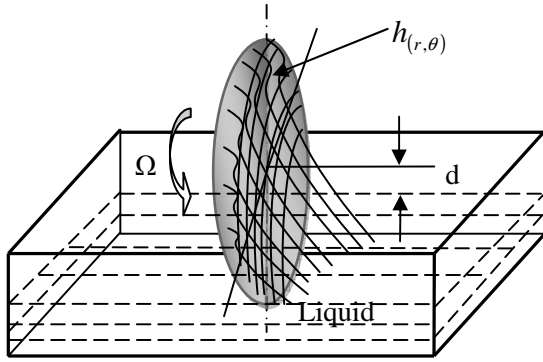


Figure 1. Configuration of a rotating disk partially immersed in liquid

Navier-Stokes equations which are used to describe the thin film flow on a vertically rotational disk can be expressed as:

$$\frac{\partial u_r}{\partial t} + u_r \frac{\partial u_r}{\partial r} + \frac{u_\theta}{r} \frac{\partial u_r}{\partial \theta} - \frac{u_\theta^2}{r} + u_z \frac{\partial u_r}{\partial z} = -\frac{1}{\rho} \frac{\partial p}{\partial r} + \nu \left[\frac{\partial^2 u_r}{\partial r^2} + \frac{1}{r} \frac{\partial u_r}{\partial r} + \frac{1}{r^2} \frac{\partial^2 u_r}{\partial \theta^2} + \frac{\partial^2 u_r}{\partial z^2} - \frac{2}{r^2} \frac{\partial u_\theta}{\partial \theta} - \frac{u_r}{r^2} \right] - g \sin \theta \quad (1a)$$

$$\frac{\partial u_\theta}{\partial t} + u_r \frac{\partial u_\theta}{\partial r} + \frac{u_\theta}{r} \frac{\partial u_\theta}{\partial \theta} + \frac{u_r u_\theta}{r} + u_z \frac{\partial u_\theta}{\partial z} = -\frac{1}{\rho r} \frac{\partial p}{\partial \theta} + \nu \left[\frac{\partial^2 u_\theta}{\partial r^2} + \frac{1}{r} \frac{\partial u_\theta}{\partial r} + \frac{1}{r^2} \frac{\partial^2 u_\theta}{\partial \theta^2} + \frac{\partial^2 u_\theta}{\partial z^2} + \frac{2}{r^2} \frac{\partial u_\theta}{\partial \theta} - \frac{u_r}{r^2} \right] - g \cos \theta \quad (1b)$$

$$\frac{\partial u_z}{\partial t} + u_r \frac{\partial u_z}{\partial r} + \frac{u_\theta}{r} \frac{\partial u_z}{\partial \theta} + u_z \frac{\partial u_z}{\partial z} = -\frac{1}{\rho} \frac{\partial p}{\partial z} + \nu \left[\frac{\partial^2 u_z}{\partial r^2} + \frac{1}{r} \frac{\partial u_z}{\partial r} + \frac{1}{r^2} \frac{\partial^2 u_z}{\partial \theta^2} + \frac{\partial^2 u_z}{\partial z^2} \right] \quad (1c)$$

where ρ , μ , ν and p denote, respectively, the density, dynamic viscosity, kinematic viscosity and the pressure of the liquid. The only external force acting on the thin film liquid is gravity

g. Thin film flows on the rotating disks, like other flows, should also satisfy the continuity, which gives

$$\frac{1}{r} \left[\frac{\partial}{\partial r} (r u_\theta) \right] + \frac{1}{r} \frac{\partial u_\theta}{\partial \theta} + \frac{\partial u_z}{\partial z} = 0 \quad (2)$$

For the boundary condition at the surface of the disk, i.e. $z=0$, no-slip condition is imposed and the disk surface is assumed to be impermeable. Thus,

$$u_r = 0, \quad u_\theta = r\Omega, \quad u_z = 0 \quad (3)$$

The total rate of change of the thin film thickness should be equal to zero, which results in the following kinematic condition

$$\frac{\partial h}{\partial t} = u_z - u_r \frac{\partial h}{\partial r} - \frac{1}{r} u_\theta \frac{\partial h}{\partial \theta} \quad (4)$$

Integration of Equation (2) and substitution into Equation (4) by applying Leibnitz integration rule yields

$$\frac{\partial h}{\partial t} = -\frac{1}{r} \frac{\partial}{\partial r} r \int_0^h u_r dz - \frac{1}{r} \frac{\partial}{\partial \theta} \int_0^h u_\theta dz \quad (5)$$

At the thin film surface, $z = h(r, \theta, t)$, the static pressure should balance the surface tension force, which requires the normal stress condition to satisfy

$$\vec{n} \cdot \mathbf{\Pi} \cdot \vec{n} = 2\sigma \quad (6)$$

while at the interface of the free surface, if the friction due to the induced air flow is neglected, the tangential stresses on the free surface of the film should disappear, which yields

$$\vec{n} \cdot \mathbf{\Pi} \cdot \vec{t}_i = 0 \quad (i = 1, 2) \quad (7)$$

The normal and the tangential vectors in radial and angular direction can be found if the thickness of the thin film can be determined based on

$$\vec{n} = \frac{\left(-\frac{\partial h}{\partial r}, -\frac{1}{r} \frac{\partial h}{\partial \theta}, 1 \right)}{\left(1 + \left(\frac{\partial h}{\partial r} \right)^2 + \frac{1}{r^2} \left(\frac{\partial h}{\partial \theta} \right)^2 \right)^{1/2}}, \quad \vec{t}_1 = \frac{\left(1, 0, \frac{\partial h}{\partial r} \right)}{\left(1 + \frac{1}{r^2} \left(\frac{\partial h}{\partial \theta} \right)^2 \right)^{1/2}}, \quad \vec{t}_2 = \frac{\left(0, 1, \frac{1}{r} \frac{\partial h}{\partial \theta} \right)}{\left(1 + \frac{1}{r^2} \left(\frac{\partial h}{\partial \theta} \right)^2 \right)^{1/2}} \quad (8)$$

while the stress tensor $\mathbf{\Pi}$ is defined and given by

$$\Pi = \begin{pmatrix} \Pi_{rr} & \Pi_{r\theta} & \Pi_{rz} \\ \Pi_{\theta r} & \Pi_{\theta\theta} & \Pi_{\theta z} \\ \Pi_{zr} & \Pi_{z\theta} & \Pi_{zz} \end{pmatrix} = \begin{pmatrix} -p + 2\mu \frac{\partial u_r}{\partial r} & \mu \left(\frac{1}{r} \frac{\partial u_r}{\partial \theta} + \frac{\partial u_r}{\partial r} - \frac{u_\theta}{r} \right) & \mu \left(\frac{\partial u_z}{\partial r} + \frac{\partial u_r}{\partial z} \right) \\ \mu \left(\frac{1}{r} \frac{\partial u_r}{\partial \theta} + \frac{\partial u_r}{\partial r} - \frac{u_\theta}{r} \right) & -p + 2\mu \left(\frac{1}{r} \frac{\partial u_\theta}{\partial \theta} + \frac{u_r}{r} \right) & \mu \left(\frac{\partial u_\theta}{\partial z} + \frac{1}{r} \frac{\partial u_z}{\partial \theta} \right) \\ \mu \left(\frac{\partial u_z}{\partial r} + \frac{\partial u_r}{\partial z} \right) & \mu \left(\frac{\partial u_\theta}{\partial z} + \frac{1}{r} \frac{\partial u_z}{\partial \theta} \right) & -p + 2\mu \frac{\partial u_z}{\partial z} \end{pmatrix} \quad (9)$$

For most of fluids, the surface tension σ is almost unchanged and can be assumed to be constant. Then, the mean curvature of the thin film free surface can be estimated by

$$k = \frac{1}{2} \left[\frac{1}{r} \frac{\partial}{\partial r} \frac{r \frac{\partial h}{\partial r}}{\left(1 + \frac{\partial^2 h}{\partial r^2} + \frac{1}{r^2} \frac{\partial^2 h}{\partial \theta^2} \right)^{\frac{1}{2}}} + \frac{1}{r} \frac{\partial}{\partial \theta} \frac{\frac{1}{r} \frac{\partial h}{\partial \theta}}{\left(1 + \frac{\partial^2 h}{\partial r^2} + \frac{1}{r^2} \frac{\partial^2 h}{\partial \theta^2} \right)^{\frac{1}{2}}} \right] \quad (10)$$

Substitution of equations (9) and (10) into equations (6) and (7) yields the boundary conditions for the normal stress, which can be written as

$$-p + \frac{2\mu}{1 + \left(\frac{\partial h}{\partial r} \right)^2 + \frac{1}{r^2} \left(\frac{\partial h}{\partial \theta} \right)^2} \left[\left(\frac{1}{r} \frac{\partial u_r}{\partial \theta} + \frac{\partial u_\theta}{\partial r} - \frac{u_\theta}{r} \right) \frac{1}{r} \frac{\partial h}{\partial r} \frac{\partial h}{\partial \theta} - \left(\frac{\partial r_z}{\partial r} + \frac{\partial u_r}{\partial z} \right) \frac{\partial h}{\partial r} - \left(\frac{\partial u_\theta}{\partial z} + \frac{1}{r} \frac{\partial u_z}{\partial \theta} \right) \frac{1}{r} \frac{\partial h}{\partial \theta} + \frac{\partial u_r}{\partial r} \left(\frac{\partial h}{\partial r} \right)^2 + \left(\frac{\partial u_\theta}{\partial \theta} + u_r \right) \frac{1}{r^3} \left(\frac{\partial h}{\partial \theta} \right)^2 + \frac{\partial u_z}{\partial z} \right] = \sigma \left[\frac{1}{r} \frac{\partial}{\partial r} \frac{r \frac{\partial h}{\partial r}}{\left(1 + \left(\frac{\partial h}{\partial r} \right)^2 + \frac{1}{r^2} \left(\frac{\partial h}{\partial \theta} \right)^2 \right)^{\frac{1}{2}}} + \frac{1}{r} \frac{\partial}{\partial \theta} \frac{\frac{1}{r} \frac{\partial h}{\partial \theta}}{\left(1 + \left(\frac{\partial h}{\partial r} \right)^2 + \frac{1}{r^2} \left(\frac{\partial h}{\partial \theta} \right)^2 \right)^{\frac{1}{2}}} \right] \quad (11)$$

and the tangential stress condition in radial direction

$$2 \left(\frac{\partial u_z}{\partial z} - \frac{\partial u_r}{\partial r} \right) \frac{\partial h}{\partial r} - \left(\frac{1}{r} \frac{\partial u_r}{\partial \theta} + \frac{\partial u_\theta}{\partial r} - \frac{u_\theta}{r} \right) \frac{1}{r} \frac{\partial h}{\partial \theta} + \left(\frac{\partial u_z}{\partial r} + \frac{\partial u_r}{\partial z} \right) \left(1 - \left(\frac{\partial h}{\partial r} \right)^2 \right) - \left(\frac{\partial u_\theta}{\partial z} + \frac{1}{r} \frac{\partial u_z}{\partial \theta} \right) \frac{1}{r} \frac{\partial h}{\partial r} \frac{\partial h}{\partial \theta} = 0 \quad (12)$$

and the tangential stress condition in angular direction

$$2 \left(\frac{\partial u_z}{\partial z} - \frac{1}{r} \frac{\partial u_\theta}{\partial \theta} - \frac{u_r}{r} \right) \frac{1}{r} \frac{\partial h}{\partial \theta} - \left(\frac{1}{r} \frac{\partial u_r}{\partial \theta} + \frac{\partial u_\theta}{\partial r} - \frac{u_\theta}{r} \right) \frac{\partial h}{\partial r} + \left(\frac{\partial u_\theta}{\partial z} + \frac{1}{r} \frac{\partial u_z}{\partial \theta} \right) \left(1 - \frac{1}{r^2} \left(\frac{\partial h}{\partial \theta} \right)^2 \right) - \left(\frac{\partial u_z}{\partial r} + \frac{\partial u_r}{\partial z} \right) \frac{1}{r} \frac{\partial h}{\partial r} \frac{\partial h}{\partial \theta} = 0 \quad (13)$$

Direct solution of Equation (1) together with the boundary conditions (3), (6), and (7) coupled with Equation (5), is impossible since the equations involved are highly non-linear. However, by introducing reasonable simplifications and assumptions, this set of partial differential equations can be solved at least numerically. The following section will discuss the existing analysis for the thin film flows on a vertically rotational disk (Afanasiev *et al.*, 2008) to such problem, which will be used for guidance for CFD modelling of the thin film flow on the vertically rotating disk.

NONDIMENSIONAL ANALYSIS

For the film formation on the vertically rotating disk, the use of lubrication approximation is feasible but the appropriate length scale should be considered. Obviously, the typical length scale should be R , the radius of the disk while the tangential velocity of the rotating disk, U , may be the suitable characteristic velocity scale, which is given by

$$U = R\Omega \quad (14)$$

and the time scale is chosen as

$$T = R/U \quad (15)$$

Since the liquid film formed on the surface of the rotating disk is very thin, a small parameter in the analysis can be introduced, i.e.

$$\alpha = \frac{H}{R} \ll 1 \quad (16)$$

On this basis, the following dimensionless variables can be introduced:

$$r = R\hat{r}, \quad \theta = \hat{\theta}, \quad z = H\hat{z}, \quad u_r = U\hat{u}_r, \quad u_\theta = U\hat{u}_\theta, \quad u_z = \alpha U\hat{u}_z, \quad p = P\hat{p}, \quad t = \hat{t} \quad (17)$$

The dominant viscous term is balanced with gravitational term in the u_r -momentum equation so that the characteristic height H can be scaled which yields

$$H = \sqrt{\frac{\mu U}{\rho g}} \quad (18)$$

It is expected that the pressure will compete with the dominant viscous term so that

$$P = \frac{\mu UR}{H^2} \quad (19)$$

Because the thin film involves the free surface, the surface tension plays an important role in controlling the liquid surface. It can be precluded that the following scale can be used to relate to the normal stress boundary condition, i.e.

$$P = \frac{\sigma H}{R^2} \quad (20)$$

Equating Equations (19) and (20) gives the scale for R as

$$R = \frac{H}{\left(\frac{\mu U}{\sigma}\right)^{1/3}} \quad (21)$$

When the capillary number Ca is introduced, it can be shown that Ca is small for the case of the thin film flow on the vertically rotating disk.

$$Ca = \left(\frac{\mu U}{\sigma}\right) = \left(\frac{H}{R}\right)^3 \ll 1 \quad (22)$$

It is noted that this length scale is appropriate for the thin film region away from the liquid bath. The length scale should be reconsidered for the balance of gravity and surface tension forces.

$$P = \rho g R \quad (23)$$

The pressure scale can be determined by surface tension

$$P = \sqrt{\sigma \rho g} \quad (24)$$

From equations (23) and (24) the length scale near the liquid bath can be obtained

$$R = \left(\frac{\sigma}{\rho g}\right)^{1/2} \quad (25)$$

We also define a Reynolds number, $Re = \rho UR/\mu$. Non-dimensionalising Equation (1) yields

$$\begin{aligned} \alpha^2 \text{Re} \left[\frac{\partial \hat{u}_r}{\partial \hat{t}} + \hat{u}_r \frac{\partial \hat{u}_r}{\partial \hat{r}} + \frac{\hat{u}_\theta}{\hat{r}} \frac{\partial \hat{u}_r}{\partial \hat{\theta}} - \frac{\hat{u}_\theta^2}{\hat{r}} + \hat{u}_z \frac{\partial \hat{u}_r}{\partial \hat{z}} \right] &= -\frac{\partial \hat{p}}{\partial \hat{r}} + \frac{\partial \hat{u}_r^2}{\partial \hat{z}^2} \\ -\sin \hat{\theta} + \alpha^2 \left[\frac{1}{\hat{r}} \frac{\partial}{\partial \hat{r}} \left(\hat{r} \frac{\partial \hat{u}_r}{\partial \hat{r}} \right) + \frac{1}{\hat{r}^2} \frac{\partial^2 \hat{u}_r}{\partial \hat{\theta}^2} - \frac{2}{\hat{r}^2} \frac{\partial \hat{u}_\theta}{\partial \hat{\theta}} - \frac{\hat{u}_r}{\hat{r}^2} \right] & \end{aligned} \quad (26)$$

$$\begin{aligned} \alpha^2 \text{Re} \left[\frac{\partial \hat{u}_\theta}{\partial \hat{t}} + \hat{u}_r \frac{\partial \hat{u}_\theta}{\partial \hat{r}} + \frac{\hat{u}_\theta}{\hat{r}} \frac{\partial \hat{u}_\theta}{\partial \hat{\theta}} + \frac{\hat{u}_r \hat{u}_\theta}{\hat{r}} + \hat{u}_z \frac{\partial \hat{u}_\theta}{\partial \hat{z}} \right] &= -\frac{1}{\hat{r}} \frac{\partial \hat{p}}{\partial \hat{\theta}} + \frac{\partial \hat{u}_\theta^2}{\partial \hat{z}^2} \\ -\cos \hat{\theta} + \alpha^2 \left[\frac{1}{\hat{r}} \frac{\partial}{\partial \hat{r}} \left(\hat{r} \frac{\partial \hat{u}_\theta}{\partial \hat{r}} \right) + \frac{1}{\hat{r}^2} \frac{\partial \hat{u}_\theta^2}{\partial \hat{\theta}^2} + \frac{2}{\hat{r}^2} \frac{\partial \hat{u}_r}{\partial \hat{\theta}} - \frac{\hat{u}_\theta}{\hat{r}^2} \right] & \end{aligned} \quad (27)$$

$$\begin{aligned} \alpha^2 \text{Re} \left[\frac{\partial \hat{u}_z}{\partial \hat{t}} + \hat{u}_r \frac{\partial \hat{u}_z}{\partial \hat{r}} + \frac{\hat{u}_\theta}{\hat{r}} \frac{\partial \hat{u}_z}{\partial \hat{\theta}} + \hat{u}_z \frac{\partial \hat{u}_z}{\partial \hat{z}} \right] &= -\frac{\partial \hat{p}}{\partial \hat{z}} + \alpha^2 \frac{\partial \hat{u}_z^2}{\partial \hat{z}^2} \\ + \alpha^2 \left[\frac{1}{\hat{r}} \frac{\partial}{\partial \hat{r}} \left(\hat{r} \frac{\partial \hat{u}_z}{\partial \hat{r}} \right) + \frac{1}{\hat{r}^2} \frac{\partial \hat{u}_z^2}{\partial \hat{\theta}^2} \right] & \end{aligned} \quad (28)$$

Here all variables have been non-dimensionalised. The boundary conditions at the disk, $\hat{z} = 0$, are

$$\hat{u}_r = 0, \quad \hat{u}_\theta = \hat{r}\hat{\Omega}, \quad \hat{u}_z = 0, \quad (29)$$

The boundary conditions at the free liquid surface $\hat{z} = \hat{h}(\hat{r}, \hat{\theta}, \hat{t})$ are:

$$\begin{aligned} -\hat{p} + \frac{2\alpha^2}{1 + \alpha^2 \frac{\partial^2 \hat{h}}{\partial \hat{r}^2} + \frac{\alpha^2}{\hat{r}^2} \frac{\partial^2 \hat{h}}{\partial \hat{\theta}^2}} \left[\alpha^2 \left(\frac{1}{\hat{r}} \frac{\partial \hat{u}_r}{\partial \hat{\theta}} + \frac{\partial \hat{u}_\theta}{\partial \hat{r}} - \frac{\hat{u}_\theta}{\hat{r}} \right) \frac{1}{\hat{r}} \frac{\partial \hat{h}}{\partial \hat{r}} \frac{\partial \hat{h}}{\partial \hat{\theta}} - \right. \\ \left. \left(\alpha^2 \frac{\partial \hat{u}_z}{\partial \hat{r}} + \frac{\partial \hat{u}_r}{\partial \hat{z}} \right) \frac{\partial \hat{h}}{\partial \hat{r}} - \left(\frac{\partial \hat{u}_z}{\partial \hat{z}} + \frac{\alpha^2}{\hat{r}} \frac{\partial \hat{u}_z}{\partial \hat{\theta}} \right) \frac{1}{\hat{r}} \frac{\partial \hat{h}}{\partial \hat{\theta}} \right. \\ \left. + \alpha^2 \frac{\partial \hat{u}_r}{\partial \hat{r}} \frac{\partial^2 \hat{h}}{\partial \hat{r}^2} + \alpha^2 \left(\frac{\partial \hat{u}_\theta}{\partial \hat{\theta}} + \hat{u}_r \right) \frac{1}{\hat{r}^3} \frac{\partial^2 \hat{h}}{\partial \hat{\theta}^2} + \frac{\partial \hat{u}_z}{\partial \hat{z}} \right] & \\ = \left[\frac{1}{\hat{r}} \frac{\partial}{\partial \hat{r}} \frac{\hat{r} \frac{\partial \hat{h}}{\partial \hat{r}}}{\left(1 + \alpha^2 \left(\frac{\partial \hat{h}}{\partial \hat{r}} \right)^2 + \frac{\alpha^2}{\hat{r}^2} \left(\frac{\partial \hat{h}}{\partial \hat{\theta}} \right)^2 \right)^{1/2}} + \frac{1}{\hat{r}} \frac{\partial}{\partial \hat{\theta}} \frac{\frac{1}{\hat{r}} \frac{\partial \hat{h}}{\partial \hat{\theta}}}{\left(1 + \alpha^2 \left(\frac{\partial \hat{h}}{\partial \hat{r}} \right)^2 + \frac{\alpha^2}{\hat{r}^2} \left(\frac{\partial \hat{h}}{\partial \hat{\theta}} \right)^2 \right)^{1/2}} \right] & \end{aligned} \quad (30)$$

$$\begin{aligned} 2\alpha^2 \left(\frac{\partial \hat{u}_z}{\partial \hat{z}} - \frac{\partial \hat{u}_r}{\partial \hat{r}} \right) \frac{\partial \hat{h}}{\partial \hat{r}} - \alpha^2 \left(\frac{1}{\hat{r}} \frac{\partial \hat{u}_r}{\partial \hat{\theta}} + \frac{\partial \hat{u}_\theta}{\partial \hat{r}} - \frac{\hat{u}_\theta}{\hat{r}} \right) \frac{1}{\hat{r}} \frac{\partial \hat{h}}{\partial \hat{\theta}} + \\ \left(\alpha^2 \frac{\partial \hat{u}_z}{\partial \hat{r}} + \frac{\partial \hat{u}_r}{\partial \hat{z}} \right) \left(1 - \alpha^2 \frac{\partial^2 \hat{h}}{\partial \hat{r}^2} \right) - \alpha^2 \left(\frac{\partial \hat{u}_\theta}{\partial \hat{z}} + \frac{\alpha^2}{\hat{r}} \frac{\partial \hat{u}_z}{\partial \hat{\theta}} \right) \frac{1}{\hat{r}} \frac{\partial \hat{h}}{\partial \hat{r}} \frac{\partial \hat{h}}{\partial \hat{\theta}} = 0 \end{aligned} \quad (31)$$

$$\begin{aligned} 2\alpha^2 \left(\frac{\partial \hat{u}_z}{\partial \hat{z}} - \frac{1}{\hat{r}} \frac{\partial \hat{u}_\theta}{\partial \hat{\theta}} - \frac{\hat{u}_r}{\hat{r}} \right) \frac{1}{\hat{r}} \frac{\partial \hat{h}}{\partial \hat{\theta}} - \alpha^2 \left(\frac{1}{\hat{r}} \frac{\partial \hat{u}_r}{\partial \hat{\theta}} + \frac{\partial \hat{u}_\theta}{\partial \hat{r}} - \frac{\hat{u}_\theta}{\hat{r}} \right) \frac{\partial \hat{h}}{\partial \hat{r}} + \\ \left(\frac{\partial \hat{u}_\theta}{\partial \hat{z}} + \frac{\alpha^2}{\hat{r}} \frac{\partial \hat{u}_z}{\partial \hat{\theta}} \right) \left(1 - \alpha^2 \frac{\partial^2 \hat{h}}{\partial \hat{\theta}^2} \right) - \alpha^2 \left(\alpha^2 \frac{\partial \hat{u}_z}{\partial \hat{r}} + \frac{\partial \hat{u}_r}{\partial \hat{z}} \right) \frac{1}{\hat{r}} \frac{\partial \hat{h}}{\partial \hat{r}} \frac{\partial \hat{h}}{\partial \hat{\theta}} = 0 \end{aligned} \quad (32)$$

Because α is very small, Equations (26), (27) and (28) can be simplified as

$$0 = -\frac{\partial \hat{p}}{\partial \hat{r}} + \frac{\partial^2 \hat{u}_r}{\partial \hat{z}^2} - \sin \hat{\theta} \quad (33)$$

$$0 = -\frac{\partial \hat{p}}{\hat{r} \partial \hat{\theta}} + \frac{\partial^2 \hat{u}_\theta}{\partial \hat{z}^2} - \cos \hat{\theta} \quad (34)$$

$$0 = -\frac{\partial \hat{p}}{\partial \hat{z}} \quad (35)$$

with the conditions (4-30), (4-31) and (4-32) to be simplified as

$$-\hat{p} = \frac{1}{\hat{r}} \frac{\partial}{\partial \hat{r}} \left(\hat{r} \frac{\partial \hat{h}}{\partial \hat{r}} \right) + \frac{\partial^2 \hat{h}}{\hat{r}^2 \partial \hat{\theta}^2} \quad (\hat{z} = \hat{h}) \quad (36)$$

$$\frac{\partial \hat{u}_r}{\partial \hat{z}} = 0 \quad (\hat{z} = \hat{h}) \quad (37)$$

$$\frac{\partial \hat{u}_\theta}{\partial \hat{z}} = 0 \quad (\hat{z} = \hat{h}) \quad (38)$$

Equations (33), (34) and (35) can now be solved with the boundary conditions (36), (37) and (38), also coupled with the kinematic condition for description of the thin film free surface, which is given by

$$\frac{\partial \hat{h}}{\partial \hat{t}} = -\frac{1}{\hat{r}} \frac{\partial}{\partial \hat{r}} \left(\hat{r} \int_0^{\hat{h}} \hat{u}_r d\hat{z} \right) - \frac{1}{\hat{r}} \frac{\partial}{\partial \hat{\theta}} \left(\int_0^{\hat{h}} \hat{u}_\theta d\hat{z} \right) \quad (39)$$

It can be seen from Equation (35) that p does not depend on z . When velocity components u_r and u_θ are given, the film thickness can be found through (39).

Rearranging Equations (33) and (34), integrating twice and applying boundary conditions (29), (37), (38), one can obtain

$$\frac{\partial^2 \hat{u}_r}{\partial \hat{z}^2} = \frac{\partial \hat{p}}{\partial \hat{r}} + \sin \hat{\theta} \quad (40)$$

$$\frac{\partial^2 \hat{u}_\theta}{\partial \hat{z}^2} = \frac{\partial \hat{p}}{\hat{r} \partial \hat{\theta}} + \cos \hat{\theta} \quad (41)$$

Substitution (40) and (41) into Equation (39) and integration yields

$$\frac{\partial \hat{h}}{\partial \hat{t}} = \frac{1}{\hat{r}} \frac{\partial}{\partial \hat{r}} \left[\hat{r} \frac{h^3}{3} \left(\frac{\partial \hat{p}}{\partial \hat{r}} + \sin \hat{\theta} \right) \right] + \frac{1}{\hat{r}} \frac{\partial}{\partial \hat{\theta}} \left[\frac{h^3}{3} \left(\frac{1}{\hat{r}} \frac{\partial \hat{p}}{\partial \hat{\theta}} + \cos \hat{\theta} \right) \right] - \hat{\Omega} \hat{r} \hat{h} \quad (42)$$

Equation (42) is the standard equation for film thickness, where

$$\hat{\Omega} = \frac{\mu \Omega}{\sqrt{\rho g \sigma}}$$

It should be noted that boundary conditions (36) to (38) is only appropriate far away from the liquid bath. If the length scale is reconsidered in the vicinity of the liquid bath as shown in Equation (25) based on the analysis by (Afanasiev *et al.*, 2008), then boundary condition (36) becomes

$$-\hat{p} = \frac{1}{\hat{r}} \frac{\partial}{\partial \hat{r}} \frac{\hat{r} \frac{\partial \hat{h}}{\partial \hat{r}}}{\left(1 + \left(\frac{\partial \hat{h}}{\partial \hat{r}} \right)^2 + \frac{1}{r^2} \left(\frac{\partial \hat{h}}{\partial \hat{\theta}} \right)^2 \right)^{\frac{1}{2}}} + \frac{1}{\hat{r}} \frac{\partial}{\partial \hat{\theta}} \frac{\frac{1}{\hat{r}} \frac{\partial \hat{h}}{\partial \hat{\theta}}}{\left(1 + \left(\frac{\partial \hat{h}}{\partial \hat{r}} \right)^2 + \frac{1}{r^2} \left(\frac{\partial \hat{h}}{\partial \hat{\theta}} \right)^2 \right)^{\frac{1}{2}}} \quad (\hat{z} = \hat{h}) \quad (43)$$

Surface tension force has a significant influence on film thickness profiles and Equation (42) needs to be solved in conjunction with Equation (43), which can be written as

$$\frac{\partial \hat{h}}{\partial \hat{t}} = \frac{1}{\hat{r}} \frac{\partial}{\partial \hat{r}} \left[-\hat{r} \frac{2h^3}{3} \left(\frac{\partial k}{\partial \hat{r}} + \sin \hat{\theta} \right) \right] + \frac{1}{\hat{r}} \frac{\partial}{\partial \hat{\theta}} \left[-\frac{2h^3}{3} \left(\frac{1}{\hat{r}} \frac{\partial k}{\partial \hat{\theta}} + \cos \hat{\theta} \right) - \hat{\Omega} \hat{r} \hat{h} \right] \quad (44)$$

where κ is curvature of free surface. Direct solution of Equation (2-44) is not possible as this kind of equation is highly non-linear. For steady thin film flow, Equation (2-44) can be further simplified as

$$\frac{1}{\hat{r}} \frac{\partial}{\partial \hat{r}} \left[-\hat{r} \frac{2h^3}{3} \left(\frac{\partial k}{\partial \hat{r}} + \sin \hat{\theta} \right) \right] + \frac{1}{\hat{r}} \frac{\partial}{\partial \hat{\theta}} \left[-\frac{2h^3}{3} \left(\frac{1}{\hat{r}} \frac{\partial k}{\partial \hat{\theta}} + \cos \hat{\theta} \right) - \hat{\Omega} \hat{r} \hat{h} \right] = 0 \quad (45)$$

CFD modelling of the thin film flow on a vertically rotational disk

Since the governing equations used to describe the thin film flow problem in current study are highly non-linear, seeking for full analytical solutions for the problem is impractical. Thus, CFD modelling approach has been adopted in this study [9,10,11]. The use of a high quality mesh and reasonable boundary conditions which are incorporated into CFD modelling is crucial to this study [12]. For the numerical solution of the thin film free surface flow, CFD code - Fluent has been used.

For the fully three dimensional problem of the rotating disk, a cylindrical coordinate system is employed where the rotating disk is placed in the middle of a cylindrical vessel to rotate vertically about the horizontal axis. Following the work done by Afanasiev *et al.* (2008), the disk radius is assumed to be $R=27.23$ mm. The length of the cylindrical vessel should be long enough and far away from the disk so that the boundary condition, $\partial/\partial z = 0$ can be imposed when the cylindrical vessel is partly filled with liquid. The cylindrical vessel has a diameter

of 80 mm and a length of 40 mm. Since the film formed on the rotational disk is very thin, a fine mesh is required in the vicinity of the disk. As shown in Figure 2, a structured grid with hexahedral elements was generated with map face meshes on the circular surfaces, extended by the cooper volume mesh to avoid numerical diffusion as much as possible. The total number of mesh used in the CFD modelling is 369,714. The use of a refined mesh was also tested but the simulation results seem to be independent of the mesh.

Volume of Fluid method (VOF) has been recognised as an appropriate numerical technique for tracking and locating the free surface of two or more immiscible fluids by calculating the volume fractions in each cell of a fixed Eulerian grid [13,14]. A volume fraction parameter F for each of the Eulerian grid is defined in the VOF method. A cell is assumed to be completely filled with liquid when $F=1$, while empty when $F=0$ and it contains interface of two or more phases if $0<F<1$. Such function F can be transported by using the advection equation. Based on F values, the free surface shape can be determined using a particular interpolation technique. VOF method is employed in current study for tracking the location and the pattern of the thin film on the vertically rotating disk.

One important feature of the VOF method is transient simulation, i.e. unsteady simulation. Thus, the simulation itself requires a careful selection of the time step so that the simulation is stable. The criterion used for determining the time step is so-called Courant number. In fact, both real fluid flow and numerical simulation of thin film flow requires that the free surface front advance cannot exceed a mesh interval. This Courant-Friedrichs-Lewy condition (CFL condition) is a necessary condition for convergence while solving certain partial differential equations numerically. The CFL condition is expressed as

$$\frac{U \Delta t}{\Delta x} \leq C \quad (46)$$

where U is the liquid velocity, Δt is the time step and Δx is the mesh interval or mesh size. Obviously, $U \Delta t < \Delta x$ should be ensured in all unsteady simulation to keep stability. In this case, a small courant number has been used, which gives a minimum time step about 10^{-3} s.

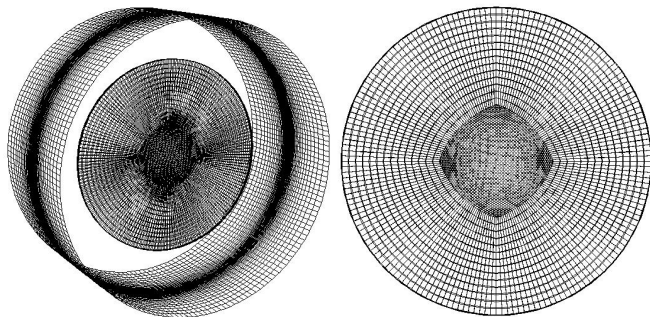


Figure 2. Grid generation for the rotating disk

NUMERICAL RESULTS AND DISCUSSION

The CFD simulations have been conducted based on four fluids of different viscosities as shown in table 1. The properties of the test fluid have been taken the same as Afanasiev *et. al.* (2008), for comparison of the simulation results.

Table 1. Different fluid properties

	μ (Pa.s)	σ (N/m)	ρ (kg/m ³)
Test fluid	1	0.0727	1000
PDMS-1	1	0.0211	975
PDMS-2	5	0.0211	975
PDMS-3	10	0.0211	975

In the simulations, the disk is assumed to rotate at a constant angular velocity Ω while it is half immersed in liquid, i.e. $d' = 0$, the immersion depth d is nondimensionalised here by dividing with the radius of the disk. In Afanasiev's *et. al.* work [1], the film thickness profile is only the function of r . However, our CFD simulation results have clearly indicated that the actual film thickness is not only dependent on r but also θ . For case of liquid being dragged out of a bath pool via a vertically moving upwards flat plate, Landau and Levich (1942) have showed that if the capillary number Ca is small, the film thickness can be estimated by

$$h = 0.93 \left(\frac{\mu U}{\rho g} \right)^{1/2} (Ca)^{1/6} \quad (47)$$

where h is the film thickness, U is the velocity of the plate, ρ is density, g is gravitational force and μ is the dynamic viscosity of the liquid. Wilson (1982) indicated that the approximate solution given by Landau and Levich (1942) is only valid when the capillary number approaches to zero and he obtained a general solution of the film thickness when the flat plate is vertically aligned, which is expressed

$$h = \left(\frac{\mu U}{\rho g} \right)^{1/2} \left[0.94581 (Ca)^{1/6} - 0.10685 (Ca)^{1/2} \right] \quad (48)$$

By using similar analysis for thin flow on vertically rotating disk, Afanasiev *et. al.* [1] obtained a steady state solution of the film thickness, which is given by

$$h = 0.94581 \left(\frac{\mu r \Omega}{\sqrt{\rho g \sigma}} \right)^{3/2} \quad (49)$$

The calculated film thickness distribution at different radial positions is shown in Figure 3, the dimensionless radius of the rotating disk is taken as $R'=10$. The comparisons are shown at $R'=9, 7, 5$ and 3 . It can be seen from Figure 3 that the film formation can be characterised by two regions (indicated in Figure 4), $0^\circ < \theta < 90^\circ$ as the region for the film drag out and $90^\circ < \theta < 180^\circ$ as the region for the film to be dragged in [15]. It was revealed from the simulation that the film is thick and

unstable in the drag-out point and it gradually becomes stable but the film has a tendency of downwards and significantly affected by all the forces acting on the film flow. The force balance may play a leading role in controlling the film flow. The forces such as viscous force, inertia, gravitational force and surface tension force acting on the film flow on the rotating disk have been discussed by [16, 17, 18]. It has been indicated from the simulation that the viscous force is dominant in the drag-out region while the gravitational force is dominant in the drag-in region.

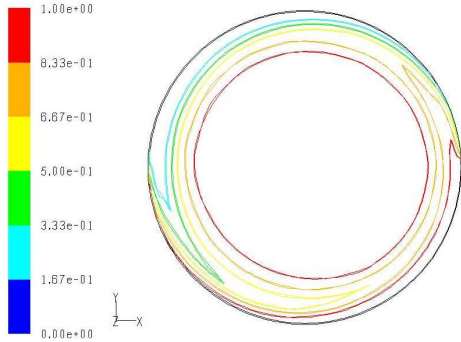


Figure 3. Film thickness profiles at different radial positions

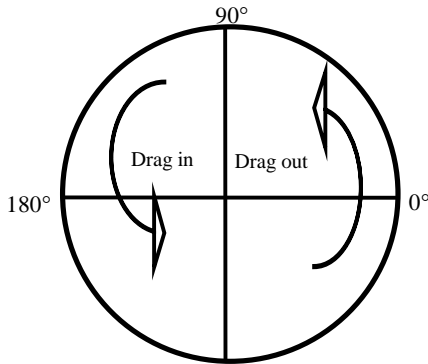


Figure 4. Drag out and drag in region

Vijayaraghan and Gupta [19] obtained a correlation for the film thickness formed on a vertically rotating disk partially immersed in Newtonian liquid based on their experimental results, which reads

$$h = \frac{7.99Ca^{2.93}\eta^{0.15}\mathfrak{X}^{5.23}}{Cas^{3.09}\chi^{0.024}} \quad (50)$$

where η is dimensionless surface tension number, \mathfrak{X} is dimensionless depth, χ is dimensionless gravitational number and Cas is modified capillary number. It can be seen clearly from equation (50) that the effect of angular position θ is not included in the correlation. However, it has been revealed from the simulation that the thin film thickness profile does depend on angular position θ as shown in Figure 5.

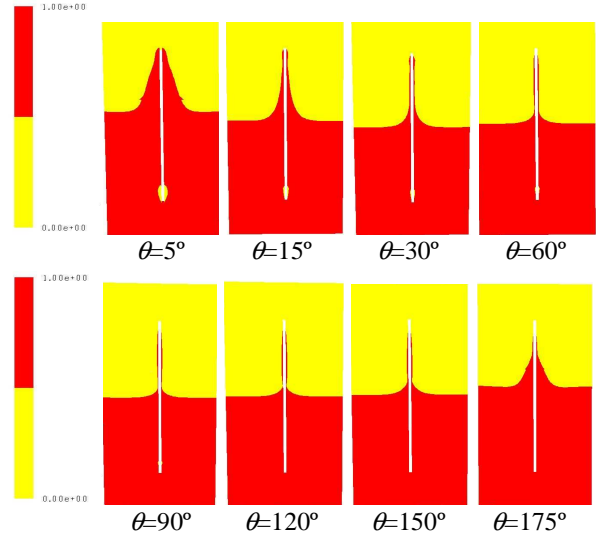


Figure 5. Drag-out and drag-in of thin film at different angular positions

It should be noted that except for the regions where the film just starts to form and re-enters the liquid, the change in the thin film thickness is not remarkable ($15^\circ < \theta < 170^\circ$) though a slight variation in film thickness is observed as can be seen from Figure-5. Figure 6 shows the variations of film thickness at different angular positions for given radius. Notice that the film thickness is non dimensionalised by dividing the radius of the disk and multiplied by a factor of 10 in all cases to contrast more clearly to reflect the structure of the film patterns.

In order to correlate the simulation results, dimensional analysis was conducted. The film thickness is dependent on a number of parameters and a functional relationship may be assumed.

$$h(r, \theta) = F(\rho, \mu, \sigma, g, \Omega, t, d, r, \theta) \quad (51)$$

where ρ is the density of the fluid, μ is the dynamic viscosity, σ is the surface tension, g is the gravitational acceleration, Ω is the rotating speed, t is the flow time, d is the immersion depth of the liquid, r is the radius, and θ is the angular position. Since previous studies on thin film flow have clearly indicated that the thin film flow can be well characterised by the following dimensionless parameters like Capillary number (Ca), Froude number (Fr), Reynolds number (Re) and Weber number (We), the functional relation (51) is assumed to be able to expressed as

$$h' = k_0 Re^{k_1} Ca^{k_2} Fr^{k_3} We^{k_4} F(t)F(d) \quad (52)$$

where h' is the dimensionless film thickness, k_0, k_1, k_2, k_3, k_4 are empirical constants which can be determined from the best regression fitting to the simulation results.

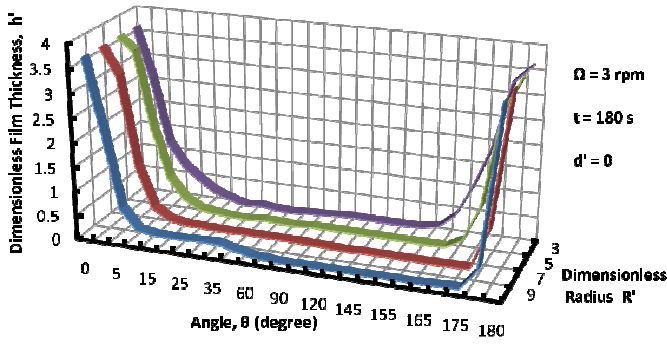


Figure 6. Film thickness at different radial and angular positions

The CFD simulation results as shown in Figure 6 can be curve-fitted using the least square technique to minimise the total error. It has been found through the trials that a combination of exponential and polynomial curve fitting can deliver the best curve fit, which is given by

$$h_{\theta} = ae^{-x_{1}\theta} + b_0 + b_1\theta + b_2\theta^2 + b_3\theta^3 + b_4\theta^4 + ce^{x_2\theta} \quad (53)$$

where, the coefficients $x_1, x_2, a, b_0, b_1, b_2, b_3, b_4,$ and c have been obtained from the CFD simulation results for any given radius. The predicted film thickness at different angular positions for given radius is now well expressed based on expression (53).

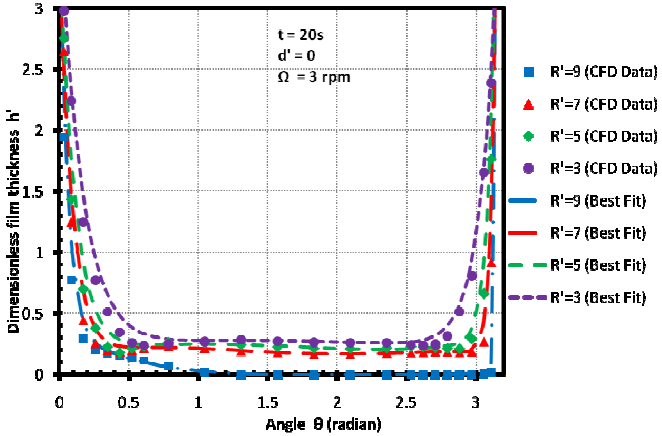


Figure 7. Film thickness at different radial direction

It can be seen from Figure 7 that the film thickness decreases from the central core towards the fringe of the disk. This is due to the gravitation force action which drives the film downward. However, as mentioned earlier, the film thickness varies along the circumferential direction. Based on our simulation results, the following fitted expression for a given radius $R'=7$ is obtained, which is given by

$$h_{\theta} = 3.48e^{-10.63\theta} + 0.06 + 0.52\theta - 0.55\theta^2 + 0.22\theta^3 - 0.03\theta^4 + 2 * 10^{-40} e^{29.48\theta} \quad (54)$$

Equation (52) has clearly indicated that the film thickness is affected by rotational speed, which has been confirmed in our simulations, as can be seen from Figure 8. The simulations were also compared with the asymptotic solutions of Afanasiev *et al.*[1] and the CFD results are consistent with the solutions as obtained by Afanasiev *et al.*[1], which has been shown in Figure 9.

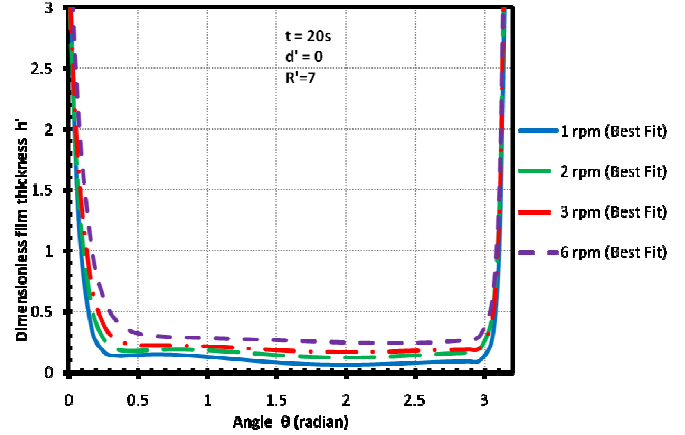


Figure 8. Film thickness at different rotational speed

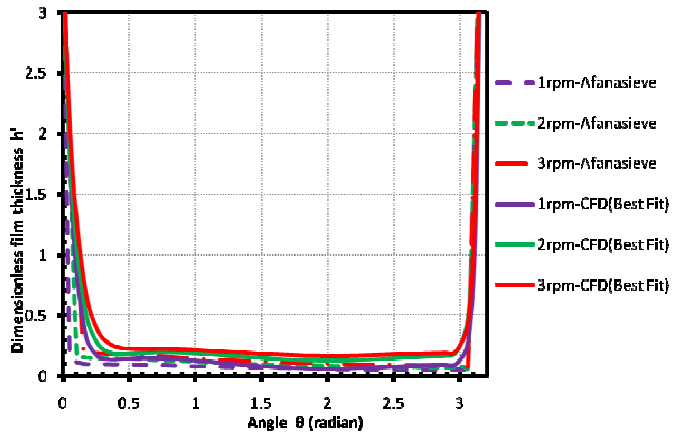


Figure 9. Comparison of the film thickness profile

It can be seen from Figure 9 that there exist difference between the film thickness profile predicted by CFD modelling and that obtained by Afanasiev *et al.* [1] in the drag-out and drag-in regions. The reason for this difference is still unclear but very likely, the solution as obtained by Afanasiev *et al.*[1] does not fully reflect the influence of the surface tension while our CFD modelling has employed the full Navier-Stokes equations for the problem. This requires further investigation.

The influence of immersion depth on the formed film thickness was also assessed in our CFD simulations. Figure 10 shows the film thickness distributions for three different immersion depths. It is interesting to note here that except for the regions of drag-out and drag in; the film thickness only slightly changes for different immersion depths which are in contradiction to the results as obtained by Afanasiev *et al.* (2008). One of

explanations is that the immersion depth only affects the drag out boundary conditions but the film flow on upper part of the rotational disk is only affected by the overall acting force balance.

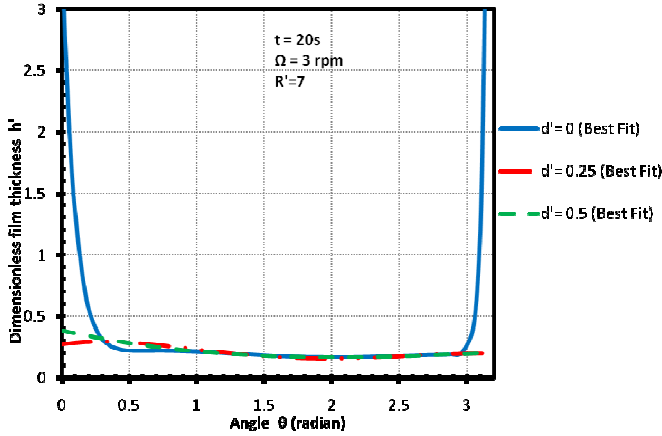


Figure 10. Film thickness at different immersion depths

The film formation on vertically rotating disk is obviously time dependent. Figure 11 shows the CFD results for the film thickness variation along the circumferential direction at given radius $R'=7$. It can be seen from Figure 11 that the film thickness profile is almost same for different flow time of the liquid. When flow time is long enough, the film flow becomes steady. Thus, for a given immersion depth, correlation (52) may be simplified as

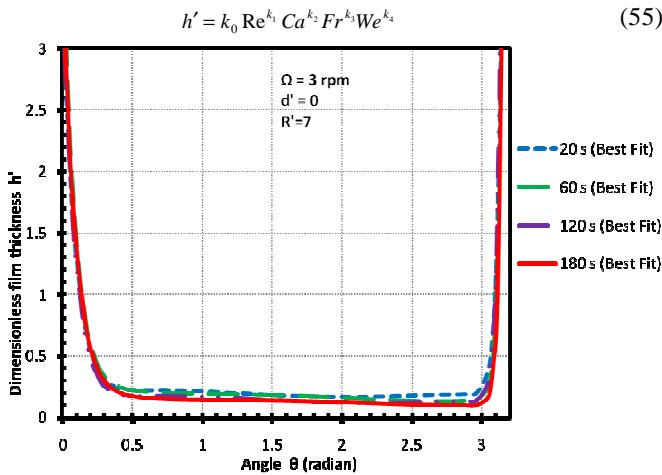


Figure 11. Film thickness at different flow time

In order to assess the influence of viscosity on the film flow behaviour, four different fluids of different viscosities have been selected in the CFD modelling. The density for PDMS-1, PDMS-2 and PDMS-3 is 975 kg/m^3 . By using correlation (55) for best fitting to the simulations, it was found that k_0, k_1, k_2, k_3, k_4 take the following values. $k_0=1.08 \times 10^9, k_1=10.204, k_2=-14.922, k_3=6.536, k_4=-4.00$.

Thus, the calculated film thickness can be estimated by

$$h' = \frac{1.08 \times 10^9 \text{ Re}^{10.204} Fr^{6.536}}{Ca^{14.922} We^{4.00}} \quad (56)$$

Figure 12 shows the predicted film thickness profiles using correlation relationship (56). It can be seen from Figure 12 that the film thickness significantly changes and becomes thicker when the liquid viscosity increases. This can be seen clearly from equation (49) since the film thickness is proportional to the viscosity to power $3/2$.

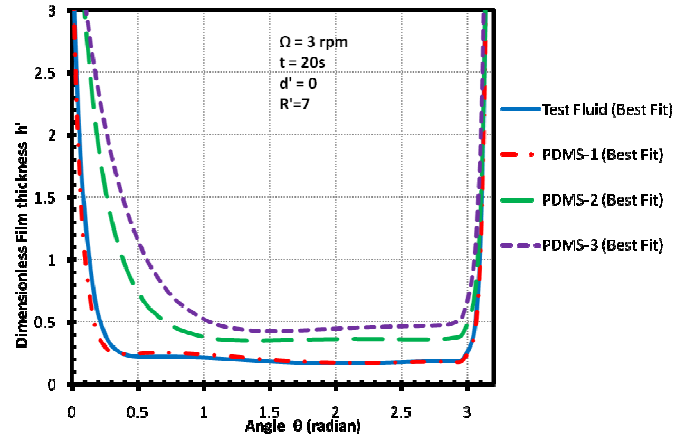


Figure 12. Effect of viscosity on film thickness profiles

CONCLUSION

The problem of the film formation on the vertically rotational disk partially immersed in liquid has been solved numerically to obtain the thin film thickness distributions. Based on CFD simulation results, a correlation is proposed to describe the film thickness distribution by defining the dominating factors controlling the thin film flows. It was found from the simulation that the two main dominant factors controlling the film thickness profile are the viscosity and rotational angular velocity. The film thickness increases significantly with increase of the angular velocity of the disk, consistent with the findings as reported in the published literature [1]. The change in the film thickness and the shape of the thin film can be characterized by the Froude number. The simulation also indicates that an increase in the viscosity causes the average film thickness to increase, indicating Capillary number and Reynolds number to be the important dimensionless parameters in thin film flow analysis. In addition, the effect of the surface tension on the film thickness profile can be indicated by incorporating the Webber number. The correlation which matches the simulation results requires introduction of a position factor to account for the change in the film thickness profile in different angular positions of the rotating disk.

REFERENCES

- [1] Afanasiev K., Munch A. and Wagner B., Thin film dynamics on a vertically rotating disk partially immersed in a liquid bath, *App. Math. Modelling*, Vol. 32, 2008, pp. 1894–1911.
- [2] Parmar N.H., Tirumkudulu M.S. and Hinch E.J., Coating flow of viscous Newtonian liquids on a rotating vertical disk, *Physics of Fluids*, Vol. 21, 2009, 103102.
- [3] Danish M., Sharma R.K., and Ali S., Gas absorption with first order chemical reaction in a laminar falling film over a reacting solid wall, *App. Math. Modelling*, Vol. 32, 2008, pp. 901–929.
- [4] Landau L. and Levich B., Dragging of a liquid by a moving plate, *Acta Physicochim. URSS*, Vol. 17, 1942, pp. 42–54.
- [5] Wilson S.D.R., The drag-out problem in film coating theory, *J. Eng. Math*, Vol. 16, 1982, pp. 209–221.
- [6] Emslie A.G., Bonner F.T. and Peck L.G., Flow of a viscous liquid on a rotating disk, *J. Appl. Phys.*, Vol. 29, 1958 pp. 858–862.
- [7] Myers T.G. and Charpin J.P.F., The effect of the Coriolis force on axisymmetric rotating thin film flows, *Int. J. of Non-Linear Mechanics*, Vol. 36, 2001, pp. 629–635.
- [8] Myers T.G. and Lombe M., The importance of the Coriolis force on axisymmetric horizontal rotating thin film flows, *Chem. Engg. and Processing*, Vol. 45, 2006, pp. 90–98.
- [9] Lan H., Friedrich M., Armaly B.F. and Drallmeier J.A., Simulation and measurement of 3D shear-driven thin liquid film flow in a duct, *Int. J. of Heat and Fluid Flow*, Vol. 29, 2008, pp. 449–459.
- [10] Aubin J., Fletcher D.F. and Xuereb C., Design of micro mixers using CFD modelling, *Chem. Eng. Science*, Vol. 60, 2005, pp. 2503 – 2516.
- [11] Hasan N. and Naser J., Determining the thickness of liquid film in laminar condition on a rotating drum surface using CFD, *Chem. Eng. Science*, Vol. 64, 2009, pp. 919 – 924.
- [12] Kim J., Adaptive Mesh Refinement for Thin Film Equations, *Journal of the Korean Physical society*, Vol. 49(5), 2006, pp. 1903 – 1907.
- [13] Gao D., Morley N.B. and Dhir V., Numerical simulation of wavy falling film flow using VOF method, *J of Comp. Physics*, Vol. 192, 2003, pp. 624–642.
- [14] Haroun Y., Legendre D. and Raynal L., Volume of fluid method for interfacial reactive mass transfer: Application to stable liquid film, *Chem. Eng. Science*, Vol. 65, 2010, pp. 2896 – 2909.
- [15] Kheshgi H. S., Kistler S. F. and Scriven L. E., Rising and falling film flows: viewed from a first-order approximation, *Chem. Eng. Science*, Vol. 47(3), 1992, pp. 683–694.
- [16] Yu S.H., Lee K.S., and Yook S.J., Film flow around a fast rotating roller, *Int. J. of Heat and Fluid Flow*, Vol. 30, 2009, pp. 796–803.
- [17] Matar O.K. and Lawrence C.J., The effect of surfactant on the flow of a thin liquid film over a spinning disc, *Chem. Eng. Science*, Vol. 61, 2006, pp. 1074 – 1091.
- [18] Krechetnikove R. and Homsy G. M., Surfactant effects in the Landau–Levich problem, *J. Fluid Mech.*, Vol. 559, 2006, pp. 429–450.
- [19] Vijayraghvan K. and Gupta J.P., Thickness of the film on a vertically rotating disk partially immersed in Newtonian liquid, *Ind. Eng. Chem. Fundam*, Vol. 21, 1982, pp. 333–336.